NASA Technical Paper 1623

Prediction Method for Two-Dimensional Aerodynamic Losses of Cooled Vanes Using Integral Boundary-Layer Parameters

Louis J. Goldman and Raymond E. Gaugler

FEBRUARY 1980

NASA

NASA Technical Paper 1623

Prediction Method for Two-Dimensional Aerodynamic Losses of Cooled Vanes Using Integral Boundary-Layer Parameters

Louis J. Goldman and Raymond E. Gaugler
Lewis Research Center
Cleveland, Ohio

SUMMARY

A generalized analysis to predict the two-dimensional aerodynamic losses of full-film-cooled vanes by using integral boundary-layer parameters is presented herein. Heat-transfer and trailing-edge injection effects are included in the method. An approximate solution of the generalized equations, for constant-static-pressure mixing, is also presented. This solution allows the effect of the different boundary-layer and cooling parameters on the losses to be seen more clearly. The analytical predictions are compared with experimental results obtained for full-film-cooled vanes at primary- to coolant-total-temperature ratios of 1 and 2.7.

The calculated loss for a full-film-cooled vane tested at the design total-temperature ratio of 2.7 agreed well with the experimental results. The variation in losses when different cooled regions of a full-film-cooled vane were tested at a total-temperature ratio of 1 was also well predicted. The boundary-layer parameters obtained from a finite-difference analysis incorporating an injection model appear well suited for use in determining the aerodynamic losses of cooled vanes. The boundary-layer analysis might be further improved by determining the effect of the free-stream pressure gradient on the injection model constants. For constant-static-pressure mixing, the calculated aerodynamic losses were approximately proportional to twice the momentum thickness minus the total enthalpy thickness at the trailing edge (for a coolant- to primary-total-pressure ratio of 1).

INTRODUCTION

Larger use of cooling air in advanced aircraft engines is necessitated by a continuing trend to higher turbine-inlet temperatures. Ongoing studies at the NASA Lewis Research Center are determining the effect of this cooling air on the turbine aerodynamic and heat-transfer characteristics. Under this program, the major effects have been identified and are summarized in reference 1. In addition, this program has provided a large experimental data base for use in developing analytical prediction techniques. Several prediction methods are presently available and have been summarized in reference 2.

Jet mixing theories (such as refs. 3 and 4) and boundary-layer injection concepts (such as refs. 5 and 6) are the types of methods most often used to predict the effect of cooling air on aerodynamic performance. Other investigators (refs. 7 and 8) have employed both mixing and boundary-layer concepts to predict the heat-transfer character-

istics of film-cooled blading. No single, unified theory that predicts both the aerodynamic losses and the heat-transfer characteristics is presently available. A method of estimating two-dimensional aerodynamic profile losses by using integral boundary-layer parameters (ref. 9) has long been in use and holds the potential of providing this unified approach. However, this method was developed for solid (uncooled) vanes and cannot in its present form be used for cooled vanes, where heat transfer occurs.

Generalization of the prediction method of reference 9 to include heat-transfer and coolant injection effects is one of the primary objectives of this report. Of equal importance, however, is the need to determine if the boundary-layer parameters obtained from a finite-difference technique (ref. 7) can be used to predict the experimental aerodynamic losses with this generalized theory. Lastly, a better understanding of the effect of heat transfer and coolant injection on the aerodynamic losses is desired.

Derivation of the generalized equations needed to predict the two-dimensional aerodynamic characteristics of film-cooled vanes by using integral boundary-layer parameters is presented herein. Modeling of trailing-edge coolant injection and heat-transfer effects is incorporated in these generalized equations. An approximate solution, assuming constant-static-pressure mixing, is also provided so that the effect of the different boundary-layer and coolant parameters on the losses can be seen more readily. Nondimensional boundary-layer characteristics for typical full-film-cooled vanes are presented, and the calculated losses for the vanes are compared with the experimental results reported in references 10 and 11.

ANALYSIS

For solid (uncooled) vanes the two-dimensional aerodynamic loss characteristics can be estimated from the vane boundary-layer parameters at the trailing edge by the method described in reference 9. In this procedure the profile losses at the vane trailing edge and the losses after the flow has mixed to uniform conditions are obtained from the displacement, momentum, kinetic energy, and trailing-edge thicknesses. For cooled vanes, where heat transfer occurs, this method (ref. 9) is not applicable since it assumes that the total temperature at the trailing edge is constant. The analysis presented herein uses the energy equation to account for heat-transfer effects and can therefore be considered a generalization of the method of reference 9. The basic flow model and assumptions used in the theory are described in the next section.

Flow Model and Assumptions

A schematic sketch of a cooled vane is shown in figure 1, together with the nomenclature used in the analysis. The flow is considered to be two dimensional. At the vane inlet, station 0, the entering flow is assumed to be uniform and at constant total pressure p_0' and total temperature T_0'. (All symbols are defined in appendix A.) The injected coolant flow is assumed to remain within the boundary layers formed on the vanes. Just downstream of the vane trailing edge, station 1, profiles of total pressure p_1' and total temperature T_1' occur due to the vane friction and the injection of coolant at a total pressure and temperature different from those of the free stream. At station 1, the static pressure p_1 and flow angle α_1 are assumed to be constant, as in reference 9. As shown in figure 1, trailing-edge coolant injection at station 1 is also allowed for. The aerodynamic loss based on kinetic energy $\overline{e}_1$ contains the vane profile losses and the losses due to coolant injection. Uniform conditions exist at station 2, where complete mixing is assumed to have taken place. The conservation of mass, momentum, and energy is applied between stations 1 and 2 to obtain the aftermixed state. This procedure is presented in appendix B. The aftermixed loss $\overline{e}_2$ contains not only the vane profile losses and the losses due to coolant injection but also the mixing losses. The aerodynamic loss coefficients $\overline{e}_1$ and $\overline{e}_2$ are calculated from the boundary-layer parameters in appendix B and summarized in the next subsection.

Loss Characteristics

Generalized analysis. - The aerodynamic performance of vanes is commonly defined as a loss coefficient based on kinetic energy (ref. 12). In equation form,

$$\overline{e} = 1 - \frac{KE}{(KE)_{id}} \tag{1}$$

where the ideal kinetic energy for cooled vanes is usually based on the sum of the coolant and primary (or main stream) kinetic energies. The loss coefficients $\overline{e}_1$ and $\overline{e}_2$ defined in terms of boundary-layer parameters at the trailing edge are presented in appendix B and are summarized here. For station 1,

$$\overline{e}_1 = 1 - \frac{1 - \overline{\delta}^* - \overline{\delta}_{te} - \overline{\psi} + K_{te}\overline{\delta}_{sl}}{\left(1 - \overline{\delta}^* - \overline{\delta}_{te} + B_{te}\overline{\delta}_{sl}\right)\left[1 - y_c + y_c\left(\dfrac{V_{c,id}}{V_{pr,id}}\right)_1^2\right]} \tag{B45a}$$

3

$$y_c = \frac{m_c}{m_T} = \frac{1 - \dfrac{T'_2}{T'_0}}{1 - \dfrac{T'_c}{T'_0}} \qquad \text{if} \quad T'_c \neq T'_0 \tag{B37}$$

$$\frac{T'_2}{T'_0} = \frac{1 - \overline{\delta}^* - \overline{\delta}_{te} - \overline{\delta}_H + E_{te}\overline{\delta}_{sl}}{1 - \overline{\delta}^* - \overline{\delta}_{te} + B_{te}\overline{\delta}_{sl}} \tag{B24}$$

And for station 2,

$$\overline{e}_2 = 1 - \frac{\left(\dfrac{V}{V_{cr}}\right)_2^2}{(1 - y_c)\left(\dfrac{V_{pr,id}}{V_{cr}}\right)_2^2 + y_c\left(\dfrac{V_{c,id}}{V_{cr}}\right)_2^2} \tag{B35a}$$

$$\left(\frac{V}{V_{cr}}\right)_2^2 = \left(\frac{V_x}{V_{cr}}\right)_2^2 + \left(\frac{V_u}{V_{cr}}\right)_2^2 \tag{B29}$$

$$\left(\frac{V_x}{V_{cr}}\right)_2 = \frac{\gamma C}{\gamma + 1} - \sqrt{\left(\frac{\gamma C}{\gamma + 1}\right)^2 - 1 + \frac{\gamma - 1}{\gamma + 1}D^2} \tag{B33}$$

$$D = \left(\frac{V_u}{V_{cr}}\right)_2 = \sqrt{\frac{1 - \overline{\delta}^* - \overline{\delta}_{te} + B_{te}\overline{\delta}_{sl}}{1 - \overline{\delta}^* - \overline{\delta}_{te} - \overline{\delta}_H + E_{te}\overline{\delta}_{sl}}} \left[\frac{\left(1 - \overline{\delta}^* - \overline{\delta}_{te} - \overline{\theta} + J_{te}\overline{\delta}_{sl}\right)\left(\dfrac{V}{V_{cr}}\right)_{fs,1} \sin \alpha_1}{1 - \overline{\delta}^* - \overline{\delta}_{te} + B_{te}\overline{\delta}_{sl}}\right]$$

$$\tag{B31}$$

4

$$C = \sqrt{\dfrac{1 - \overline{\delta}^* - \overline{\delta}_{te} + B_{te}\overline{\delta}_{sl}}{1 - \overline{\delta}^* - \overline{\delta}_{te} - \overline{\delta}_H + E_{te}\overline{\delta}_{sl}}}$$

$$\times \left\{ \dfrac{\left(1 - \overline{\delta}^* - \overline{\delta}_{te} - \overline{\theta} + J_{te}\overline{\delta}_{sl}\right)\left(\dfrac{V}{V_{cr}}\right)^2_{fs,1} \cos^2\alpha_1 + \dfrac{\gamma+1}{2\gamma}\left[1 - \dfrac{\gamma-1}{\gamma+1}\left(\dfrac{V}{V_{cr}}\right)^2_{fs,1}\right]}{\left(1 - \overline{\delta}^* - \overline{\delta}_{te} + B_{te}\overline{\delta}_{sl}\right)\left(\dfrac{V}{V_{cr}}\right)_{fs,1} \cos\alpha_1} \right\}$$

(B28)

where the ideal velocity ratios $\left(V_{pr,id}/V_{cr}\right)_2$ and $\left(V_{c,id}/V_{cr}\right)_2$ are calculated from the static pressure p_2 as determined in appendix B. The loss coefficients $\overline{e}_1$ and $\overline{e}_2$ are complicated functions of the boundary-layer parameters $\overline{\delta}^*$, $\overline{\theta}$, $\overline{\delta}_H$, and $\overline{\psi}$; the trailing-edge coolant injection parameters B_{te}, J_{te}, E_{te}, and K_{te}; and the trailing-edge geometry $\overline{\delta}_{te}$ and $\overline{\delta}_{sl}$. They are also functions of the critical velocity ratio $\left(V/V_{cr}\right)_{fs,1}$ and the flow angle α_1. The effect of heat transfer (total-temperature profile at the trailing edge) is contained in the parameter $\overline{\delta}_H$, which is defined as the total enthalpy thickness. The above relationships for the loss coefficient simplify considerably if certain approximations are made. These approximations are discussed in the next subsection since they allow the effects of the boundary-layer and cooling parameters on the losses to be seen more readily.

Constant-static-pressure mixing approximation. – The assumption that the static pressures at stations 1 and 2 (fig. 1) are the same has been used by other investigators (refs. 13 and 14) to simplify the solution of the mixing equations. Further approximations are also possible once it is realized that the boundary-layer parameters $\overline{\delta}^*$, $\overline{\theta}$, $\overline{\delta}_H$, $\overline{\psi}$, $\overline{\delta}_{te}$, and $\overline{\delta}_{sl}$ are often much less than 1. With these approximations, it is shown in appendix C that for typical first-stage operating conditions (i.e., equal vane-coolant and primary-flow total pressures) the loss coefficients are

$$\overline{e}_1 \approx \overline{\psi} + \overline{\psi}_{te} - \left(\overline{\delta}_H + \overline{\delta}_{H,te}\right) \qquad \text{if } T'_c \neq T'_0 \text{ and } p'_c = p'_0 \qquad \text{(C17)}$$

$$\overline{e}_2 \approx 2\left(\overline{\theta} + \overline{\theta}_{te}\right) - \left(\overline{\delta}_H + \overline{\delta}_{H,te}\right) \qquad \text{if } T'_c \neq T'_0 \text{ and } p'_c = p'_0 \qquad \text{(C13)}$$

5

These particularly simple expressions indicate that the losses $\bar{e}_1$ and $\bar{e}_2$ depend directly on the kinetic energy thicknesses $\bar{\psi}$ and $\bar{\psi}_{te}$, the momentum thicknesses $\bar{\theta}$ and $\bar{\theta}_{te}$, and the total enthalpy thicknesses $\bar{\delta}_H$ and $\bar{\delta}_{H,te}$, but not on the displacement thickness $\bar{\delta}^*$ or the trailing-edge thickness $\bar{\delta}_{te}$. There are two terms for each thickness because there is a loss due to the boundary layer formed along the vane surface and an additional loss due to coolant injected at the trailing edge.

The total enthalpy thicknesses $\bar{\delta}_H$ and $\bar{\delta}_{H,te}$ are defined so that they are positive if the coolant total temperature is less than the main-stream total temperature. It would appear from equations (C17) and (C13) that coolant injection tends to decrease the losses through the total enthalpy thicknesses. However, the total-temperature profile caused by the coolant injection also tends to increase the kinetic energy and momentum thicknesses. Therefore, it is not possible to determine from equations (C17) and (C13) how the losses change with coolant addition. This must be done by the boundary-layer calculation.

The change in the losses $\Delta\bar{e}$ (between stations 1 and 2) defined as

$$\Delta\bar{e} = \bar{e}_2 - \bar{e}_1 \approx 2\left(\bar{\theta} + \bar{\theta}_{te}\right) - \left(\bar{\psi} + \bar{\psi}_{te}\right) \tag{C18}$$

can be shown (appendix C) to be always greater than zero. That is, there is always a mixing loss in going from station 1 to station 2.

The approximate relations presented in this section are intended to show the effect of the different boundary-layer parameters on the losses in a simple manner and are not recommended for calculation of the loss coefficients. The general expressions summarized previously and given in detail in appendix B should be used.

Boundary-Layer Parameters

An analysis that accurately predicts the boundary-layer parameters is obviously required to use the method presented in appendix B for predicting the aerodynamic losses of cooled vanes. One boundary-layer method that allows for discrete-hole coolant injection is described in reference 7. As this method is used in the next section to calculate the aerodynamic performance of a typical full-film-cooled vane, it is briefly described here. The method of reference 7 uses a two-dimensional, finite-difference, boundary-layer calculation for the solid surface combined with a model of the injection process. The calculations proceed in the streamwise direction until a row of holes is encountered. At this point the finite-difference calculations stop and fluid is injected into the boundary layer.

In the injection model, a fraction of the coolant is assumed to remain in each stream tube as the coolant passes through the stream tubes comprising the boundary layer. This fraction of coolant is then mixed at constant static pressure with the boundary-layer mass in the stream tube. This process continues in successive stream tubes until all the coolant is added to the boundary layer. The distance at which this occurs is called the penetration distance. In addition, the injectant and the boundary layer interact and thus increase the turbulence level in the boundary layer. This process is modeled by increasing the value of Prandtl's mixing length over that which would occur without injection. The maximum mixing length is assumed to occur at the injectant penetration distance.

The two constants in this injection model (one constant determines the penetration distance and the other the maximum mixing length) were determined experimentally in reference 7 as a function of the mass-flux ratio $(\rho V)_c / (\rho V)_{fs}$ for 30° slant-hole injection on a flat plate. After the injection process is completed, the finite-difference calculations resume with the new boundary-layer profile and continue until another row of holes is encountered.

The boundary conditions must be known or estimated to calculate the boundary-layer parameters by the method of reference 7. For cooled vanes the boundary conditions needed are the streamwise variation in free-stream conditions V_{fs}, the streamwise variation in wall temperature T_w, and the flow conditions of the coolant $\rho_c V_c$ and T'_c at the exit of the injection holes. The first of these boundary conditions could be estimated from a two-dimensional, potential flow solution (e.g., ref. 15); the latter boundary conditions could be obtained from a heat-transfer analysis (e.g., ref. 16).

In general, these types of analyses would be a part of the design procedure for a cooled vane and would therefore not require additional effort. They do, however, introduce some uncertainty into the determination of the boundary-layer parameters. To circumvent this difficulty in this report, experimental results were selected (refs. 10 and 11) in which most of the boundary conditions were measured. That is, not only was the aerodynamic performance measured, but so were the vane static-pressure distribution, the coolant flow rates, and the wall temperature distribution. These boundary conditions were used in the boundary-layer analysis (ref. 7) to determine the boundary-layer parameters. The boundary-layer parameters were then used in the prediction method (appendix B) to determine the aerodynamic performance. The results of these calculations for a typical full-film-cooled vane are presented in the next section.

RESULTS AND DISCUSSION

Description of Film-Cooled Vane

The experimental aerodynamic performance of a typical full-film-cooled core vane has been presented in references 10 and 11 for tests conducted at primary- to coolant-total-temperature ratios T_0'/T_c' of 1 and 2.7, respectively. The vane profile and the cooling-hole pattern (fig. 2) were the same for both tests. For the measurements of reference 10, however, the vane insert was not used and the hole diameters were different. Also shown in figure 2(b) is the nomenclature of the film-cooled regions tested individually or in combination in reference 10. That is, experimental performance was obtained when the following regions (fig. 2(b)) of the vane were film cooled: (1) pressure surface, region P; (2) diffusing part of suction surface, region D; (3) full suction surface, region AD; (4) trailing edge, region T; (5) pressure surface and accelerating part of suction surface and trailing edge, region PAT; and (6) full vane, region PADT. The solid (uncooled) vane is designated S.

The free-stream critical velocity ratio distribution for the vane (calculated from measured static pressures) is shown in figure 3, together with the interpolated values used in the boundary-layer program. This velocity distribution, particularly on the suction surface, has a large influence on the development of the boundary-layer parameters along the vane. Before the performance of the vanes is discussed, the calculated boundary-layer characteristics for the different film-cooled regions are presented.

Boundary-Layer Characteristics

Primary- to coolant-total-temperature ratio of 1. - The streamwise variation in momentum-thickness Reynolds number $(Re)_\theta$ for the different film-cooled regions (tested in ref. 10) is shown in figures 4 and 5 for the pressure and suction surfaces, respectively. The term $(Re)_\theta$ is used herein because it is the criterion set in the boundary-layer program for the start of transition from laminar to turbulent flow.

For the solid (uncooled) vane S, a conservative value of 200 for $(Re)_\theta$ (ref. 12) was assumed for the start of transition. According to this criterion, the boundary layer (fig. 4(a)) remains laminar over most of the pressure surface (fig. 4(a)) but is turbulent over most of the suction surface (fig. 5(a)). Comparing the pressure and suction surfaces at the trailing edge indicates that the $(Re)_\theta$ (or momentum thickness θ) for the suction surface is almost seven times larger than that for the pressure surface. Since the losses $\bar{e}_2$ were shown to be approximately proportional to the momentum thickness (for $y_c = 0$ or $T_0'/T_c' = 1$, $\bar{\delta}_H = \bar{\delta}_{H,te} = 0$), the suction surface contributes most of the losses.

For the film-cooled regions shown in figures 4(b), 5(b), 5(c), and 5(d), transition was assumed to be triggered by the coolant injection at the first row of holes, provided that $(Re)_\theta$ was less than 200. The discontinuities in the figures occur at each row of cooling holes and are the result of the constant-static-pressure mixing of the coolant with the boundary layer. Injection on the pressure surface P (fig. 4(b)) more than triples the momentum thickness at the trailing edge over that at the solid pressure surface. This is due, in part, to the assumed triggering of turbulent flow by the coolant injection. The momentum thickness, however, is still much less than the value for the solid suction surface (fig. 5(a)). Injection on the accelerating part of the suction surface A (fig. 5(b)) increases the trailing-edge momentum thickness by only about 20 percent. On the other hand, injection on the diffusion region D (fig. 5(c)) or on the full suction surface AD (fig. 5(d)) more than doubles the momentum thickness over that of the solid surface (fig. 5(a)). They are also over six to seven times larger than for the cooled pressure surface P. Therefore, as for the solid vane, the losses for the full-film-cooled vane PAD are largely controlled by the suction-surface momentum thickness.

Primary- to coolant-total-temperature ratio of 2.7. - The momentum-thickness Reynolds number $(Re)_\theta$ and total-enthalpy-thickness Reynolds number $(Re)_{\delta_H}$ are shown in figures 6 and 7 for the full-film-cooled pressure and suction surfaces, respectively. Only the full-film-cooled vane PADT was tested at the higher total-temperature ratio. For injection on the pressure surface P (fig. 6), the total enthalpy thickness (at the trailing edge) is slightly less than twice the momentum thickness. Since the losses are approximately equal to twice the momentum thickness minus the total enthalpy thickness, the pressure surface again contributes little to the total losses. For the cooled suction surface AD (fig. 7), however, the total enthalpy and momentum thicknesses are about equal. Therefore, the losses for the full-film-cooled vane PADT are again controlled mainly by the losses on the suction surface. The calculated and measured losses are compared in the next section.

Comparison of Calculated and Measured Losses

The calculated aftermixed loss coefficients $\overline{e}_2$ are compared with the experimental results in figure 8 for tests conducted at primary- to coolant-total-temperature ratios T'_0/T'_c of 1 (ref. 10) and 2.7 (ref. 11), respectively. The single experimental value shown in figure 8(b) was determined from the mean-radius survey data presented in reference 11. In figure 8, the difference in the bar graphs or in the experimental points, between the film-cooled and solid vane, represents the losses incurred in cooling that region of the vane surface. Since the calculated and experimental losses for the solid (uncooled) vane agree so well, a direct comparison of the experimental point

and bar graph for any cooled region shows how well the effect of the cooling on the losses is predicted. For all the film-cooled regions tested, the calculated and experimental losses agree quite well, with an average deviation of ±0.003. This value compares well with the generally quoted experimental accuracy in $\bar{e}_2$ of ±0.0025 for solid (uncooled) vanes; this value would be expected to be somewhat higher for cooled vanes.

It is, therefore, concluded that the effect of film cooling on the aerodynamic losses can be predicted to an accuracy comparable to that with which it can be measured. However, if the cooled region contains the diffusing part of the suction surface (i.e., D, AD, and PADT), the calculated losses are slightly higher than measured. Similarly, for the accelerating regions (i.e., P and PAT) the calculated losses are slightly lower than measured. The reason for this is not known, but it may be due to the effect of pressure gradient on the constants in the boundary-layer coolant injection model. As discussed in the section ANALYSIS, these constants were determined from flat-plate (zero pressure gradient) coolant injection tests. It is, therefore, felt that the boundary-layer analysis may be further improved by determining the effect of free-stream pressure gradient on the injection model constants.

As noted previously, the effect of cooling the different regions of the vane can be inferred from figure 8 by comparing the cooled-region losses with each other and with the solid (uncooled) vane losses. For example, the loss due to cooling the accelerating part of the suction surface, region A, is smaller than the loss due to cooling the diffusion part of the suction surface, region D. This is, of course, the same result arrived at previously by comparing the boundary-layer characteristics. Because region A was not tested individually, there is no data point shown in figure 8 (a) for this region. The calculated losses are shown in figure 8 (a) since the boundary-layer parameters were needed to calculate the losses for region PAT. Other regions not tested (i.e., region PDT) could have just as easily been shown in figure 8 (a). The point is that calculating the losses is relatively simple once the boundary-layer parameters for the different cooled regions have been determined. In fact, the boundary-layer parameters are easily obtained for different cooled regions and could be used to optimize the design of cooled vanes.

SUMMARY OF RESULTS

A generalized analysis to predict the two-dimensional aerodynamic losses of full-film-cooled vanes by using integral boundary-layer parameters has been presented herein. Heat-transfer and trailing-edge injection effects are included in the method. An approximate solution of the generalized equations, for constant-static-pressure mixing, has also been presented. This solution allows the effect of the different boundary-layer and cooling parameters on the losses to be seen more readily. The analytical

predictions are compared with the experimental results obtained for full-film-cooled vanes tested at primary- to coolant-total-temperature ratios of 1 and 2.7. The following results were obtained:

1. The calculated loss for a full-film-cooled vane tested at the design total-temperature ratio of 2.7 agreed well with experimental results. The variation in losses when different cooled regions of a full-film-cooled vane were tested at a total-temperature ratio of 1 was also well predicted.

2. The boundary-layer parameters obtained from a finite-difference analysis incorporating an injection model appear well suited for use in determining the aerodynamic losses of cooled vanes. The boundary-layer analysis might be further improved by determining the effect of free-stream pressure gradient on the injection model constants.

3. For constant-static-pressure mixing, the calculated aerodynamic losses were approximately proportional to twice the momentum thickness minus the total enthalpy thickness at the trailing edge (for a coolant- to primary-total-pressure ratio of 1).

Lewis Research Center,
    National Aeronautics and Space Administration,
        Cleveland, Ohio, October 5, 1979,
            505-04.

APPENDIX A

SYMBOLS

B_{te} ratio of trailing-edge-coolant to free-stream mass flux, $(\rho V)_{c,te}/(\rho V)_{fs,1}$

C parameter defined in eq. (B28)

C_p specific heat at constant pressure, J/kg K

D parameter defined in eq. (B31)

E_{te} ratio of trailing-edge-coolant to free-stream energy flux,

     $(\rho VT')_{c,te}/(\rho VT')_{fs,1}$

$\bar{e}$ loss coefficient based on kinetic energy, $1 - (KE/KE_{id})$

H total enthalpy, J/kg

J_{te} ratio of trailing-edge-coolant to free-stream momentum flux,

     $\left(\rho V^2\right)_{c,te}/\left(\rho V^2\right)_{fs,1}$

KE kinetic energy, $\frac{1}{2}mV^2$, J/sec

K_{te} ratio of trailing-edge-coolant to free-stream kinetic energy flux,

     $\left(\rho V^3\right)_{c,te}/\left(\rho V^3\right)_{fs,1}$

m mass flow rate, kg/sec

p pressure, N/m^2

R gas constant, J/kg K

$(Re)_{\delta_H}$ total-enthalpy-thickness Reynolds number, $\rho V_{fs}\delta_H/\mu$

$(Re)_\theta$ momentum-thickness Reynolds number, $\rho V_{fs}\theta/\mu$

s vane spacing, m

sl trailing-edge slot width (fig. 1), m

T temperature, K

t trailing-edge thickness (fig. 1), m

u tangential direction of cascade, m

V velocity, m/sec

x axial direction of cascade, m

y_c coolant mass-flow fraction, m_c/m_T

α flow angle measured from axial direction, deg

γ ratio of specific heats

δ boundary-layer thickness, m

δ^* displacement thickness, $\displaystyle\int_0^\delta \left(1 - \frac{\rho_1 V_1}{(\rho V)_{fs,1}}\right) d\eta$, m

δ_H total enthalpy thickness, $\displaystyle\int_0^\delta \frac{\rho_1 V_1}{(\rho V)_{fs,1}} \left(1 - \frac{T_1'}{T_{fs,1}'}\right) d\eta$, m

$\overline{\delta}^*$ $(\delta_s^* + \delta_p^*)/(s \cos \alpha_1)$

$\overline{\delta}_H$ $(\delta_{H,s} + \delta_{H,p})/(s \cos \alpha_1)$

$\overline{\delta}_{H,te}$ effective total-enthalpy thickness of trailing-edge coolant injection, eq. (C11b)

$\overline{\delta}_{sl}$ $sl/(s \cos \alpha_1)$

$\overline{\delta}_{te}$ $t/(s \cos \alpha_1)$

ϵ dimensionless parameter whose value is much less than 1

η coordinate normal to vane surface, m

θ momentum thickness, $\displaystyle\int_0^\delta \frac{\rho_1 V_1}{(\rho V)_{fs,1}} \left(1 - \frac{V_1}{V_{fs,1}}\right) d\eta$, m

$\overline{\theta}$ $(\theta_s + \theta_p)/(s \cos \alpha_1)$

$\overline{\theta}_{te}$ effective momentum thickness of trailing-edge coolant injection, eq. (C11a)

μ viscosity, kg/m sec

ξ coordinate tangent to vane surface, m

ρ density, kg/m^3

ψ kinetic energy thickness, $\displaystyle\int_0^\delta \frac{\rho_1 V_1}{(\rho V)_{fs,1}} \left(1 - \frac{V_1^2}{V_{fs,1}^2}\right) d\eta$, m

$\overline{\psi}$ $(\psi_s + \psi_p)/(s \cos \alpha_1)$

$\overline{\psi}_{te}$ effective kinetic-energy thickness of trailing-edge coolant injection, eq. (C15)

13

Subscripts:

c   coolant flow

cr   flow conditions at Mach 1

fs   free stream

id   ideal or isentropic process

p   pressure surface

pr   primary flow

s   suction surface

T   total flow (coolant plus primary)

te   trailing edge

u   tangential direction

x   axial direction

0   station at vane inlet (fig. 1)

1   station at trailing edge (fig. 1)

2   station far downstream of vane trailing edge, where flow is completely mixed to uniform (aftermixed) conditions (fig. 1)

Superscript:

$(\ )'$ total-state conditions

APPENDIX B

AERODYNAMIC LOSS COEFFICIENTS OF COOLED VANES IN TERMS

OF BOUNDARY-LAYER PARAMETERS

Aftermixed Conditions

To obtain the aerodynamic loss coefficient at station 2 the aftermixed conditions have to first be determined in terms of the boundary-layer parameters at station 1 (fig. 1). The conservation of mass, axial and tangential momentum, and energy between stations 1 and 2 results in the following equations:

$$\int_0^S \rho_1 V_{1,x} \, du = \rho_2 V_{2,x} S = m_T \tag{B1}$$

$$\int_0^S \left(\rho_1 V_{1,x}^2 + p_1 \right) du = \left(\rho_2 V_{2,x}^2 + p_2 \right) S \tag{B2}$$

$$\int_0^S \rho_1 V_{1,x} V_{1,u} \, du = \rho_2 V_{2,x} V_{2,u} S \tag{B3}$$

$$\int_0^S \rho_1 V_{1,x} H_1 \, du = \rho_2 V_{2,x} H_2 S \tag{B4}$$

The fluid is assumed to be a perfect gas with constant specific heat. Therefore,

$$\rho = \frac{p}{RT} \tag{B5}$$

$$H = C_p T' = C_p T + \frac{V^2}{2} \tag{B6}$$

To allow the use of the boundary-layer parameters at station 1, it is assumed that the static pressure p_1 and the flow angle α_1 are constant. This allows equations (B1) to (B4) to be expressed as

$$(\rho V)_{fs,1} \cos \alpha_1 \left[s - \frac{(\delta_s + \delta_p)}{\cos \alpha_1} - \frac{t}{\cos \alpha_1} \right] + \cos \alpha_1 \int_0^{\delta_s/\cos \alpha_1} \rho_1 V_1 \, du$$

$$+ (\rho V)_{c,te} sl + \cos \alpha_1 \int_0^{\delta_p/\cos \alpha_1} \rho_1 V_1 \, du = \rho_2 V_{1,x} s \qquad \text{(B7)}$$

$$\left(\rho V^2 \right)_{fs,1} \cos^2 \alpha_1 \left[s - \frac{(\delta_s + \delta_p)}{\cos \alpha_1} - \frac{t}{\cos \alpha_1} \right] + \cos^2 \alpha_1 \int_0^{\delta_s/\cos \alpha_1} \rho_1 V_1^2 \, du + \left(\rho V^2 \right)_{c,te}$$

$$\times \cos \alpha_1 sl + \cos^2 \alpha_1 \int_0^{\delta_p/\cos \alpha_1} \rho_1 V_1^2 \, du + p_1 s = \left(\rho_2 V_{2,x}^2 + p_2 \right) s \qquad \text{(B8)}$$

$$\left(\rho V^2 \right)_{fs,1} \sin \alpha_1 \cos \alpha_1 \left[s - \frac{(\delta_s + \delta_p)}{\cos \alpha_1} - \frac{t}{\cos \alpha_1} \right]$$

$$+ \sin \alpha_1 \cos \alpha_1 \int_0^{\delta_s/\cos \alpha_1} \rho_1 V_1^2 \, du + \left(\rho V^2 \right)_{c,te} \sin \alpha_1 sl$$

$$+ \sin \alpha_1 \cos \alpha_1 \int_0^{\delta_p/\cos \alpha_1} \rho_1 V_1^2 \, du = \rho_2 V_{2,x} V_{2,u} s \qquad \text{(B9)}$$

$$(\rho V T')_{fs,1} \cos \alpha_1 \left[s - \frac{(\delta_s + \delta_p)}{\cos \alpha_1} - \frac{t}{\cos \alpha_1} \right]$$

$$+ \cos \alpha_1 \int_0^{\delta_s/\cos \alpha_1} \rho_1 V_1 T_1' \, du + (\rho V T')_{c,te} sl$$

$$+ \cos \alpha_1 \int_0^{\delta_p/\cos \alpha_1} \rho_1 V_1 T_1' \, du = \rho_2 V_{2,x} T_2' s \qquad \text{(B10)}$$

Equations (B7) to (B10) assume that the flow conditions of the coolant injected at the trailing edge are uniform and that the projection of the boundary-layer thickness δ in the u-direction is equal to $\delta/\cos \alpha_1$. To transform the remaining integrals in equations (B7) to (B10) to the boundary-layer coordinate system (ξ, η), it is also necessary to

assume that ρ_1, V_1, and T_1' are independent of ξ. This is similar to the assumption made in reference 13 that the axial gradients of the flow in the boundary-layer wake are not large. With this assumption, the substitution

$$u = \frac{\eta}{\cos \alpha_1} \tag{B11}$$

in the integrals and the following boundary-layer-parameter definitions

$$\bar{\delta}^* = \frac{\delta^*_s + \delta^*_p}{s \cos \alpha_1} = \frac{1}{s \cos \alpha_1} \left\{ \int_0^{\delta_s} \left[1 - \frac{\rho_1 V_1}{(\rho V)_{fs,1}} \right] d\eta + \int_0^{\delta_p} \left[1 - \frac{\rho_1 V_1}{(\rho V)_{fs,1}} \right] d\eta \right\} \tag{B12}$$

$$\bar{\theta} = \frac{\theta_s + \theta_p}{s \cos \alpha_1} = \frac{1}{s \cos \alpha_1} \left[\int_0^{\delta_s} \frac{\rho_1 V_1}{(\rho V)_{fs,1}} \left(1 - \frac{V_1}{V_{fs,1}} \right) d\eta + \int_0^{\delta_p} \frac{\rho_1 V_1}{(\rho V)_{fs,1}} \left(1 - \frac{V_1}{V_{fs,1}} \right) d\eta \right] \tag{B13}$$

$$\bar{\delta}_H = \frac{\delta_{H,s} + \delta_{H,p}}{s \cos \alpha_1} = \frac{1}{s \cos \alpha_1} \left[\int_0^{\delta_s} \frac{\rho_1 V_1}{(\rho V)_{fs,1}} \left(1 - \frac{T_1'}{T_{fs,1}'} \right) d\eta \right.$$

$$\left. + \int_0^{\delta_p} \frac{\rho_1 V_1}{(\rho V)_{fs,1}} \left(1 - \frac{T_1'}{T_{fs,1}'} \right) d\eta \right] \tag{B14}$$

allow equations (B7) to (B10) to be expressed as

$$\left(1 - \bar{\delta}^* - \bar{\delta}_{te} + B_{te} \bar{\delta}_{sl} \right) (\rho V)_{fs,1} \cos \alpha_1 = \rho_2 V_{2,x} \tag{B15}$$

$$\left(1 - \bar{\delta}^* - \bar{\delta}_{te} - \bar{\theta} + J_{te} \bar{\delta}_{sl} \right) \left(\rho V^2 \right)_{fs,1} \cos^2 \alpha_1 + p_1 = \rho_2 V_{2,x}^2 + p_2 \tag{B16}$$

17

$$\left(1 - \bar{\delta}^* - \bar{\delta}_{te} - \bar{\theta} + J_{te}\bar{\delta}_{sl}\right)\left(\rho V^2\right)_{fs,1} \sin \alpha_1 \cos \alpha_1 = \rho_2 V_{2,x} V_{2,u} \tag{B17}$$

$$\left(1 - \bar{\delta}^* - \bar{\delta}_{te} - \bar{\delta}_H + E_{te}\bar{\delta}_{sl}\right)\left(\rho V T'\right)_{fs,1} \cos \alpha_1 = \rho_2 V_{2,x} T'_2 \tag{B18}$$

where

$$\bar{\delta}_{te} = \frac{t}{s \cos \alpha_1} \tag{B19a}$$

$$\bar{\delta}_{sl} = \frac{sl}{s \cos \alpha_1} \tag{B19b}$$

$$B_{te} = \frac{(\rho V)_{c,te}}{(\rho V)_{fs,1}} \tag{B19c}$$

$$J_{te} = \frac{\left(\rho V^2\right)_{c,te}}{\left(\rho V^2\right)_{fs,1}} \tag{B19d}$$

$$E_{te} = \frac{(\rho V T')_{c,te}}{(\rho V T')_{fs,1}} \tag{B19e}$$

To put equations (B15) to (B17) into dimensionless form, similar to those in reference 9, the following relations are used:

$$V_{cr} = \sqrt{\frac{2\gamma}{\gamma + 1} R T'} \tag{B20a}$$

$$T'_{fs,1} = T'_0 \tag{B20b}$$

$$p'_{fs,1} = p'_0 \tag{B20c}$$

with the result that

$$\left(1 - \bar{\delta}^* - \bar{\delta}_{te} + B_{te}\bar{\delta}_{sl}\right)\left(\frac{\rho V}{\rho' V_{cr}}\right)_{fs,1} \cos \alpha_1 = \left(\frac{\rho V_x}{\rho' V_{cr}}\right)_2 \frac{p'_2}{p'_0} \sqrt{\frac{T'_0}{T'_2}} \tag{B21}$$

$$\left(1 - \overline{\delta}^* - \overline{\delta}_{te} - \overline{\theta} + J_{te}\overline{\delta}_{sl}\right)\left(\frac{\rho V^2}{\rho' V_{cr}^2}\right)_{fs,1} \cos^2\alpha_1$$

$$+ \left(\frac{\gamma + 1}{2\gamma}\right)\frac{p_1}{p_0'} = \left(\frac{\rho V_x^2}{\rho' V_{cr}^2}\right)_2 \frac{p_2'}{p_0'} + \left(\frac{\gamma + 1}{2\gamma}\right)\frac{p_2}{p_0'} \qquad \text{(B22)}$$

$$\left(1 - \overline{\delta}^* - \overline{\delta}_{te} - \overline{\theta} + J_{te}\overline{\delta}_{sl}\right)\left(\frac{\rho V^2}{\rho' V_{cr}^2}\right)_{fs,1} \sin\alpha_1 \cos\alpha_1 = \left(\frac{\rho V_x V_u}{\rho' V_{cr}^2}\right)_2 \frac{p_2'}{p_0'} \qquad \text{(B23)}$$

Solving equations (B15) and (B18) gives

$$\frac{T_2'}{T_0'} = \frac{1 - \overline{\delta}^* - \overline{\delta}_{te} - \overline{\delta}_H + E_{te}\overline{\delta}_{sl}}{1 - \overline{\delta}^* - \overline{\delta}_{te} + B_{te}\overline{\delta}_{sl}} \qquad \text{(B24)}$$

Solving equation (B21) for p_2'/p_0' gives

$$\frac{p_2'}{p_0'} = \sqrt{\frac{T_2'}{T_0'}\left[\frac{\left(1 - \overline{\delta}^* - \overline{\delta}_{te} + B_{te}\overline{\delta}_{sl}\right)\left(\frac{\rho V}{\rho' V_{cr}}\right)_{fs,1} \cos\alpha_1}{\left(\frac{\rho V_x}{\rho' V_{cr}}\right)_2}\right]} \qquad \text{(B25)}$$

Substituting p_2'/p_0' from (B25) into equation (B22) and eliminating p_1/p_0' with the relation

$$\frac{p}{p'} = \left(\frac{\rho}{\rho'}\right)\left[1 - \left(\frac{\gamma - 1}{\gamma + 1}\right)\left(\frac{V}{V_{cr}}\right)^2\right] \qquad \text{(B26)}$$

gives, after simplification,

$$\left(\frac{\rho V_x^2}{\rho' V_{cr}^2}\right)_2 - C\left(\frac{\rho V_x}{\rho' V_{cr}}\right)_2 + \left(\frac{\gamma + 1}{2\gamma}\right)\frac{p_2}{p_2'} = 0 \tag{B27}$$

where the parameter C is defined as

$$C = \sqrt{\frac{1 - \bar{\delta}^* - \bar{\delta}_{te} + B_{te}\bar{\delta}_{sl}}{1 - \bar{\delta}^* - \bar{\delta}_{te} - \bar{\delta}_H + E_{te}\bar{\delta}_{sl}}}$$

$$\times \left\{ \frac{\left(1 - \bar{\delta}^* - \bar{\delta}_{te} - \bar{\theta} + J_{te}\bar{\delta}_{sl}\right)\left(\frac{V}{V_{cr}}\right)_{fs,1}^2 \cos^2\alpha_1 + \frac{\gamma+1}{2\gamma}\left[1 - \frac{\gamma-1}{\gamma+1}\left(\frac{V}{V_{cr}}\right)_{fs,1}^2\right]}{\left(1 - \bar{\delta}^* - \bar{\delta}_{te} + B_{te}\bar{\delta}_{sl}\right)\left(\frac{V}{V_{cr}}\right)_{fs,1} \cos\alpha_1} \right\}$$

$$\tag{B28}$$

By substituting for p_2/p_2' from equation (B26), and since

$$\left(\frac{V}{V_{cr}}\right)_2 = \sqrt{\left(\frac{V_x}{V_{cr}}\right)_2^2 + \left(\frac{V_u}{V_{cr}}\right)_2^2} \tag{B29}$$

equation (B27) becomes

$$\left(\frac{V_x}{V_{cr}}\right)_2^2 - C\left(\frac{V_x}{V_{cr}}\right)_2 + \frac{\gamma+1}{2\gamma}\left\{1 - \frac{\gamma-1}{\gamma+1}\left[\left(\frac{V_x}{V_{cr}}\right)_2^2 + \left(\frac{V_u}{V_{cr}}\right)_2^2\right]\right\} = 0 \tag{B30}$$

Solving equations (B21) and (B23) for $\left(V_u/V_{cr}\right)_2$ gives

20

$$\left(\frac{V_u}{V_{cr}}\right)_2 = \sqrt{\frac{1 - \overline{\delta}^* - \overline{\delta}_{te} + B_{te}\overline{\delta}_{sl}}{1 - \overline{\delta}^* - \overline{\delta}_{te} - \overline{\delta}_H + E_{te}\overline{\delta}_{sl}}}$$

$$\times \left[\frac{\left(1 - \overline{\delta}^* - \overline{\delta}_{te} - \overline{\theta} + J_{te}\overline{\delta}_{sl}\right)\left(\frac{V}{V_{cr}}\right)_{is,1}\sin\alpha_1}{1 - \overline{\delta}^* - \overline{\delta}_{te} + B_{te}\overline{\delta}_{sl}}\right] \equiv D \qquad (B31)$$

Substituting $\left(V_u/V_{cr}\right)_2 = D$ from (B31) into (B30) gives a quadratic equation for $\left(V_x/V_{cr}\right)_2$

$$\left(\frac{V_x}{V_{cr}}\right)_2^2 - \frac{2\gamma}{\gamma + 1} C\left(\frac{V_x}{V_{cr}}\right)_2 + \left(1 - \frac{\gamma - 1}{\gamma + 1}D^2\right) = 0 \qquad (B32)$$

Since the parameters C and D depend on conditions at station 1, the solution of equation (B32) is

$$\left(\frac{V_x}{V_{cr}}\right)_2 = \frac{\gamma C}{\gamma + 1} - \sqrt{\left(\frac{\gamma C}{\gamma + 1}\right)^2 - 1 + \frac{\gamma - 1}{\gamma + 1}D^2} \qquad (B33)$$

The negative root has been used in equation (B33) to give the subsonic solution for the axial critical velocity ratio.

Although the form of equation (B33) is the same as that given in reference 9, they are not identical. The differences occur in the definitions of the parameters C and D. For C and D given by equations (B28) and (B31), respectively, additional terms that account for the effect of trailing-edge coolant injection (i.e., B_{te}, J_{te}, and E_{te}) and total-temperature profile (i.e., $\overline{\delta}_H$) occur. If these terms are all zero (as for a solid vane), the definitions for C and D reduce to those given in reference 9.

Once the critical velocity ratios $\left(V/V_{cr}\right)_2$ and $\left(V_x/V_{cr}\right)_2$ are determined from equations (B29), (B31), and (B33), the pressure ratios p_2/p_2' and p_2'/p_0' can be calculated from equations (B26) and (B25), respectively, since $(\rho/\rho')_2$ is also a function of $\left(V/V_{cr}\right)_2$. The aftermixed conditions have now been determined in terms of the boundary-layer parameters at the trailing edge. The loss coefficients will be discussed next.

Loss Coefficients

Aftermixed state. – The aftermixed loss coefficient $\overline{e}_2$, based on kinetic energy, is defined as

$$\overline{e}_2 = 1 - \frac{(KE)_2}{(KE)_{id,2}} \tag{B34}$$

For the thermodynamic definition of loss coefficient the ideal kinetic energy can be written as the sum of the coolant and primary kinetic energies. Since the flow conditions are constant at station 2, equation (B34) becomes

$$\overline{e}_2 = 1 - \frac{m_T V_2^2}{m_{pr} V_{pr,id,2}^2 + m_c V_{c,id,2}^2} = 1 - \frac{\left(\dfrac{V}{V_{cr}}\right)_2^2}{(1 - y_c)\left(\dfrac{V_{pr,id}}{V_{cr}}\right)_2^2 + y_c \left(\dfrac{V_{c,id}}{V_{cr}}\right)_2^2} \tag{B35a}$$

where

$$\left(\frac{V_{pr,id}}{V_{cr}}\right)_2^2 = \frac{\gamma + 1}{\gamma - 1} \frac{T_0'}{T_2'}\left[1 - \left(\frac{p_2}{p_0'}\right)^{(\gamma-1)/\gamma}\right] \tag{B35b}$$

$$\left(\frac{V_{c,id}}{V_{cr}}\right)_2^2 = \frac{\gamma + 1}{\gamma - 1} \frac{T_c'}{T_2'}\left[1 - \left(\frac{p_2}{p_c'}\right)^{(\gamma-1)/\gamma}\right] \tag{B35c}$$

$$y_c = \frac{m_c}{m_{pr} + m_c} = \frac{m_c}{m_T} \tag{B35d}$$

When the total temperatures of the coolant and primary flow are not equal, an overall energy balance gives

$$m_c T_c' + m_{pr} T_0' = m_T T_2' \tag{B36}$$

which when solved for the coolant fraction y_c gives

$$y_c = \frac{1 - \dfrac{T'_2}{T'_0}}{1 - \dfrac{T'_c}{T'_0}} \quad \text{if } T'_c \neq T'_0 \tag{B37}$$

The loss coefficient $\bar{e}_2$ can be calculated by using the aftermixed conditions determined in the previous section.

Trailing-edge plane. – A loss coefficient at the trailing edge $\bar{e}_1$ can also be defined. It is of interest because it does not contain the mixing losses due to flow equalization. The loss coefficient $\bar{e}_1$ is defined as

$$\bar{e}_1 = 1 - \frac{(KE)_1}{(KE)_{id,1}} \tag{B38}$$

The actual kinetic energy at station 1 is obtained by integration since the velocity V_1 varies. Therefore,

$$(KE)_1 = \frac{1}{2} \int_0^S \rho_1 V_{1,x} V_1^2 \, du = \frac{1}{2} \left\{ \left[s - \frac{(\delta_p + \delta_s)}{\cos \alpha_1} - \frac{t}{\cos \alpha_1} \right] \left(\rho V^3 \right)_{fs,1} \cos \alpha_1 \right.$$

$$+ \int_0^{\delta_s/\cos \alpha_1} \rho_1 V_{1,x} V_1^2 \, du + \left(\rho V^3 \right)_{c,te} s1$$

$$\left. + \int_0^{\delta_p/\cos \alpha_1} \rho_1 V_{1,x} V_1^2 \, du \right\} \tag{B39}$$

The terms $\bar{\psi}$ and K_{te} are defined as follows:

$$\bar{\psi} = \frac{\psi_s + \psi_p}{s \cos \alpha_1} = \frac{1}{s \cos \alpha_1} \left[\int_0^{\delta_s} \frac{\rho_1 V_1}{(\rho V)_{fs,1}} \left(1 - \frac{V_1^2}{V_{fs,1}^2} \right) d\eta + \int_0^{\delta_p} \frac{\rho_1 V_1}{(\rho V)_{fs,1}} \left(1 - \frac{V_1^2}{V_{fs,1}^2} \right) d\eta \right]$$

$$\tag{B40}$$

$$K_{te} = \frac{\left(\rho V^3\right)_{c,\,te}}{\left(\rho V^3\right)_{fs,\,1}} \tag{B41}$$

Substituting into equation (B39) gives (by using eq. (B11))

$$(KE)_1 = \frac{1}{2}\left(1 - \bar{\delta}^* - \bar{\delta}_{te} - \bar{\psi} + K_{te}\bar{\delta}_{sl}\right)\left(\rho V^3\right)_{fs,\,1}\, s\, \cos\alpha_1 \tag{B42}$$

The ideal kinetic energy at station 1 is again defined as the sum of the coolant and primary kinetic energies. Since the static pressure p_1 has been assumed to be constant, the ideal kinetic energy can be expressed as

$$(KE)_{id,\,1} = \frac{1}{2}\left(m_{pr}V^2_{pr,\,id,\,1} + m_c V^2_{c,\,id,\,1}\right) = \frac{1}{2}\left[(1 - y_c)V^2_{pr,\,id,\,1} + y_c V^2_{c,\,id,\,1}\right]m_T \tag{B43}$$

Using equation (B1) for the total mass flow m_T and equation (B15) results in

$$(KE)_{id,\,1} = \frac{1}{2}\left(1 - \bar{\delta}^* - \bar{\delta}_{te} + B_{te}\bar{\delta}_{sl}\right)\left[(1 - y_c)V^2_{pr,\,id,\,1} + y_c V^2_{c,\,id,\,1}\right](\rho V)_{fs,\,1}\, s\, \cos\alpha_1 \tag{B44}$$

The loss coefficient $\bar{e}_1$ therefore is

$$\bar{e}_1 = 1 - \frac{1 - \bar{\delta}^* - \bar{\delta}_{te} - \bar{\psi} + K_{te}\bar{\delta}_{sl}}{\left(1 - \bar{\delta}^* - \bar{\delta}_{te} + B_{te}\bar{\delta}_{sl}\right)\left[1 - y_c + y_c \left(\dfrac{V_{c,\,id}}{V_{pr,\,id}}\right)^2_1\right]} \tag{B45a}$$

where

$$\left(\frac{V_{c,\,id}}{V_{pr,\,id}}\right)^2_1 = \left(\frac{V_{c,\,id}}{V_{fs}}\right)^2_1 = \frac{T'_c}{T'_0}\left[\frac{1 - \left(\dfrac{p_1}{p'_c}\right)^{(\gamma-1)/\gamma}}{1 - \left(\dfrac{p_1}{p'_0}\right)^{(\gamma-1)/\gamma}}\right] \tag{B45b}$$

APPENDIX C

CONSTANT-STATIC-PRESSURE MIXING APPROXIMATION

The assumption that the static pressures at stations 1 and 2 (fig. 1) are the same has been used by other investigators (refs. 13 and 14) to simplify the solution of the mixing equations. The mixing equations, of course, can be solved in general without this assumption. The results are presented in appendix B. The constant-static-pressure mixing approximation is used herein because it allows the effects of the boundary-layer parameter on the loss coefficients to be seen more readily. We will therefore let

$$p_1 \approx p_2 = \text{Constant} \tag{C1}$$

Solving equations (B15) and (B16) for $V_{2,x}$ gives

$$V_{2,x} \approx \frac{\left(1 - \bar{\delta}^* - \bar{\delta}_{te} - \bar{\theta} + J_{te}\bar{\delta}_{sl}\right)V_{fs,1}\cos\alpha_1}{1 - \bar{\delta}^* - \bar{\delta}_{te} + B_{te}\bar{\delta}_{sl}} \tag{C2}$$

Solving equations (B15) and (B17) for $V_{2,u}$ gives

$$V_{2,u} = \frac{\left(1 - \bar{\delta}^* - \bar{\delta}_{te} - \bar{\theta} + J_{te}\bar{\delta}_{sl}\right)V_{fs,1}\sin\alpha_1}{1 - \bar{\delta}^* - \bar{\delta}_{te} + B_{te}\bar{\delta}_{sl}} \tag{C3}$$

And the velocity V_2 is, therefore,

$$V_2 = \sqrt{V_{2,x}^2 + V_{2,u}^2} \approx \frac{V_{fs,1}\left(1 - \bar{\delta}^* - \bar{\delta}_{te} - \bar{\theta} + J_{te}\bar{\delta}_{sl}\right)}{1 - \bar{\delta}^* - \bar{\delta}_{te} + B_{te}\bar{\delta}_{sl}} \tag{C4}$$

Since the ideal velocities are

$$V_{pr,id,2} \approx V_{pr,id,1} = V_{fs,1} \tag{C5a}$$

$$V_{c,id,2} \approx V_{c,id,1} \tag{C5b}$$

the aftermixed loss coefficient $\bar{e}_2$ from equation (B35) becomes

$$\bar{e}_2 \approx 1 - \frac{\left(\dfrac{1 - \bar{\delta}^* - \bar{\delta}_{te} - \bar{\theta} + J_{te}\bar{\delta}_{sl}}{1 - \bar{\delta}^* - \bar{\delta}_{te} + B_{te}\bar{\delta}_{sl}}\right)^2}{1 - y_c + y_c \left(\dfrac{V_{c,id}}{V_{fs}}\right)^2_1} \tag{C6}$$

where $\left(V_{c,id}/V_{fs}\right)^2_1$ is given by equation (B45b).

Further approximation of equation (C6) is possible once it is recognized that the boundary-layer parameters (i.e., $\bar{\delta}^*$, $\bar{\delta}_{te}$, $\bar{\theta}$, and $\bar{\delta}_{sl}$) and the coolant fraction y_c are usually much smaller than 1. The following approximation can then be used:

$$\frac{1}{1 - \varepsilon} \approx 1 + \varepsilon \qquad \varepsilon \ll 1 \tag{C7a}$$

This assumes that ε^2 is negligible. Using equation (C7a) in equation (C6) gives (assuming ε^2 terms are zero)

$$\frac{1}{1 - \bar{\delta}^* - \bar{\delta}_{te} + B_{te}\bar{\delta}_{sl}} \approx 1 + \bar{\delta}^* + \bar{\delta}_{te} - B_{te}\bar{\delta}_{sl} \tag{C7b}$$

$$\frac{1 - \bar{\delta}^* - \bar{\delta}_{te} - \bar{\theta} + J_{te}\bar{\delta}_{sl}}{1 - \bar{\delta}^* - \bar{\delta}_{te} + B_{te}\bar{\delta}_{sl}}$$

$$\approx \left(1 - \bar{\delta}^* - \bar{\delta}_{te} - \bar{\theta} + J_{te}\bar{\delta}_{sl}\right)\left(1 + \bar{\delta}^* + \bar{\delta}_{te} - B_{te}\bar{\delta}_{sl}\right) \approx 1 - \bar{\theta} - (B_{te} - J_{te})\bar{\delta}_{sl} \tag{C7c}$$

$$\left(\frac{1 - \bar{\delta}^* - \bar{\delta}_{te} - \bar{\theta} + J_{te}\bar{\delta}_{sl}}{1 - \bar{\delta}^* - \bar{\delta}_{te} + B_{te}\bar{\delta}_{sl}}\right)^2 \approx 1 - 2\bar{\theta} - 2(B_{te} - J_{te})\bar{\delta}_{sl} \tag{C7d}$$

Therefore,

$$\bar{e}_2 \approx 2\bar{\theta} + 2(B_{te} - J_{te})\bar{\delta}_{sl} - y_c \left\{ 1 - \frac{T'_c}{T'_0}\left[\frac{1 - \left(\dfrac{p_1}{p'_c}\right)^{(\gamma-1)/\gamma}}{1 - \left(\dfrac{p_1}{p'_0}\right)^{(\gamma-1)/\gamma}}\right] \right\} \tag{C8}$$

If the coolant and primary total temperatures are not equal, equations (B37) and (B24) can be used to find the coolant fraction y_c. Using the same approximation (i.e., eq. (C7a)) gives

$$y_c \approx \frac{\overline{\delta}_H + (B_{te} - E_{te})\overline{\delta}_{sl}}{1 - \dfrac{T_c'}{T_0'}} \qquad (C9)$$

Substituting equation (C9) into equation (C8) results in

$$\overline{e}_2 \approx 2\overline{\theta} + 2(B_{te} - J_{te})\overline{\delta}_{sl} - \left[\overline{\delta}_H + (B_{te} - E_{te})\overline{\delta}_{sl}\right] \left\{ \frac{1 - \dfrac{T_c'}{T_0'}\left[\dfrac{1 - \left(\dfrac{p_1}{p_c'}\right)^{(\gamma-1)/\gamma}}{1 - \left(\dfrac{p_1}{p_0'}\right)^{(\gamma-1)/\gamma}}\right]}{1 - \dfrac{T_c'}{T_0'}} \right\} \quad \text{if } T_c' \neq T_0' \qquad (C10)$$

From the definitions of the trailing-edge coolant injection constants given in equation (B19), it can be seen that

$$(B_{te} - J_{te})\overline{\delta}_{sl} = \frac{\dfrac{(\rho V)_{c,te}}{(\rho V)_{fs,1}}\left(1 - \dfrac{V_{c,te}}{V_{fs,1}}\right)sl}{s\cos\alpha_1} \equiv \overline{\theta}_{te} \qquad (C11a)$$

and

$$(B_{te} - E_{te})\overline{\delta}_{sl} = \frac{\dfrac{(\rho V)_{c,te}}{(\rho V)_{fs,1}}\left(1 - \dfrac{T_{c,te}'}{T_{fs,1}'}\right)sl}{s\cos\alpha_1} \equiv \overline{\delta}_{H,te} \qquad (C11b)$$

where $\overline{\theta}_{te}$ and $\overline{\delta}_{H,te}$ represent the effective momentum and total-enthalpy thicknesses, respectively, of the trailing-edge coolant injection. Equation (C10) can therefore be written as

$$e_2 \approx 2\bar{\theta} + 2\bar{\theta}_{te} - \left(\bar{\delta}_H + \bar{\delta}_{H,te}\right) \left\{ \frac{1 - \dfrac{T'_c}{T'_0}\left[\dfrac{1 - \left(\dfrac{p_1}{p'_c}\right)^{(\gamma-1)/\gamma}}{1 - \left(\dfrac{p_1}{p'_0}\right)^{(\gamma-1)/\gamma}}\right]}{1 - \dfrac{T'_c}{T'_0}} \right\} \quad \text{if} \ \ T'_c \neq T'_0 \qquad \text{(C12)}$$

To a first-order approximation, the losses e_2 depend directly on the momentum and total-enthalpy thicknesses but are independent of the displacement and trailing-edge thicknesses. For the special case of equal coolant and primary total pressures $(p'_c = p'_0)$, which is typical for first-stage cooled turbine vanes, equation (C12) becomes simply

$$e_2 \approx 2\left(\bar{\theta} + \bar{\theta}_{te}\right) - \left(\bar{\delta}_H + \bar{\delta}_{H,te}\right) \quad \text{if} \ \ T'_c \neq T'_0 \ \text{ and } \ p'_c = p'_0 \qquad \text{(C13)}$$

The losses at the trailing-edge plane $\bar{e}_1$ can also be approximated by using equation (C7a), which when applied to equation (B45a) gives in a similar manner

$$\bar{e}_1 \approx \bar{\psi} + (B_{te} - K_{te})\bar{\delta}_{sl} - \left[\bar{\delta}_H + (B_{te} - E_{te})\bar{\delta}_{sl}\right] \left\{ \frac{1 - \dfrac{T'_c}{T'_0}\left[\dfrac{1 - \left(\dfrac{p_1}{p'_c}\right)^{(\gamma-1)/\gamma}}{1 - \left(\dfrac{p_1}{p'_0}\right)^{(\gamma-1)/\gamma}}\right]}{1 - \dfrac{T'_c}{T'_0}} \right\} \quad \text{if} \ \ T'_c \neq T'_0$$

$$\text{(C14)}$$

But

$$(B_{te} - K_{te})\bar{\delta}_{sl} = \frac{\dfrac{(\rho V)_{c,te}}{(\rho V)_{fs,1}}\left(1 - \dfrac{V_{c,te}^2}{V_{fs,1}^2}\right)sl}{s \cos \alpha_1} \equiv \bar{\psi}_{te} \qquad (C15)$$

Therefore,

$$\bar{e}_1 \approx \bar{\psi}' + \bar{\psi}_{te} - \left(\bar{\delta}_H + \bar{\delta}_{H,te}\right)\left\{\frac{1 - \dfrac{T_c'}{T_0'}\left[\dfrac{1 - \left(\dfrac{p_1}{p_c'}\right)^{(\gamma-1)/\gamma}}{1 - \left(\dfrac{p_1}{p_0'}\right)^{(\gamma-1)/\gamma}}\right]}{1 - \dfrac{T_c'}{T_0'}}\right\} \quad \text{if } T_c' \neq T_0' \qquad (C16)$$

For equal coolant and primary total pressures this reduces to

$$\bar{e}_1 \approx \left(\bar{\psi}' + \bar{\psi}_{te}\right) - \left(\bar{\delta}_H + \bar{\delta}_{H,te}\right) \quad \text{if } T_c' \neq T_0' \text{ and } p_c' = p_0' \qquad (C17)$$

The change in loss $\Delta\bar{e}$ between stations 1 and 2 is defined as

$$\Delta\bar{e} = \bar{e}_2 - \bar{e}_1 \approx 2\left(\bar{\theta} + \bar{\theta}_{te}\right) - \left(\bar{\psi} + \bar{\psi}_{te}\right) \qquad (C18)$$

which is true, in general, without restrictions on T_c' or p_c'. But

$$2\bar{\theta}_{te} - \bar{\psi}_{te} = \frac{(\rho V)_{c,te}}{(\rho V)_{fs,1}}\left(1 - \frac{V_{c,te}}{V_{fs,1}}\right)^2 \frac{sl}{s \cos \alpha_1} \qquad (C19a)$$

and

$$2\bar{\theta} - \bar{\psi} = \frac{\displaystyle\int_0^{\delta_s} \frac{\rho_1 V_1}{(\rho V)_{fs,1}} \left(1 - \frac{V_1}{V_{fs,1}}\right)^2 d\eta + \int_0^{\delta_p} \frac{\rho_1 V_1}{(\rho V)_{fs,1}} \left(1 - \frac{V_1}{V_{fs,1}}\right)^2 d\eta}{s \cos \alpha_1} \tag{C19b}$$

Since these terms (i.e., eqs. (C19a) and (C19b)) are always greater than zero, the change in loss $\Delta\bar{e}$ is

$$\Delta\bar{e} > 0 \tag{C20}$$

and represents the mixing loss in going from station 1 to station 2.

Note that the approximations presented in this appendix are not recommended for the calculation of the loss coefficients. The general expressions derived in appendix B should be used. The equations presented in appendix C are intended to show the effect of the different boundary-layer and cooling parameters on the losses in a simple, but approximate, manner.

REFERENCES

1. Moffitt, Thomas P.; Stepka, Francis S.; and Rohlik, Harold E.: Summary of NASA Aerodynamic and Heat Transfer Studies in Turbine Vanes and Blades. SAE Paper 760917, Nov. 1976. (Also NASA TM X-73518, 1976.)

2. McFarland, E.; and Tabakoff, W.: An Analytical Method for Predicting the Aerodynamic Performance of a Turbine Cascade with Film Cooling. (Cincinnati Univ.; NASA Grant NGR-36-004-064.) NASA CR-135175, 1977.

3. Prust, Herman W., Jr.: An Analytical Study of the Effect of Coolant Flow Variables on the Kinetic Energy Output of a Cooled Turbine Blade Row. AIAA Paper 72-12, Jan. 1972. (Also NASA TM X-67960, 1971.)

4. Hartsel, J. E.: Prediction of Effects of Mass-Transfer Cooling on the Blade-Row Efficiency of Turbine Airfoils. AIAA Paper 72-11, Jan. 1972.

5. Tabakoff, W.; and Earley, R.: Two-Dimensional Flow Losses of a Turbine Cascade with Boundary Layer Injection. ASME Paper 72-GT-46, Mar. 1972.

6. Zimmerman, D. R.; Bennett, W. A.; and Herring, H. J.: Aerodynamic Loss Analysis for Quasi-Transpiration Cooled Turbine Blades. EDR 7796, Detroit Diesel Allison, 1973.

7. Crawford, M. E.; Kays, W. M.; and Moffat, R. J.: Heat Transfer to a Full-Coverage Film-Cooled Surface with 30° Slant-Hole Injection. NASA CR-2786, 1976.

8. Kruse, Heinz: Fundamental Investigations of Effusion Cooling of Turbine Blades. ESA-TT-469, European Space Agency, Paris, Apr. 1978.

9. Stewart, Warner L.: Analysis of Two-Dimensional Compressible-Flow Loss Characteristics Downstream of Turbomachine Blade Rows in Terms of Boundary-Layer Characteristics. NACA TN 3515, 1955.

10. Kline, John F.; Stabe, Roy G.; and Moffitt, Thomas P.: Effect of Cooling-Hole Geometry on Aerodynamic Performance of a Film-Cooled Vane Tested with Cold Air in a Two-Dimensional Cascade. NASA TP-1136, 1978.

11. McDonel, J. D.; et al.: Core Turbine Aerodynamic Evaluation-Test Data from Initial Turbine. NASA CR-2596, 1976.

12. Glassman, Arthur J., ed.: Turbine Design and Application. NASA SP-290, Vols. 1, 2, 3, 1972.

13. Lieblein, Seymour; and Roudebush, William H.: Theoretical Loss Relations for Low-Speed Two-Dimensional Cascade Flow. NACA TN 3662, 1956.

14. Vavra, Michael H.: Aero-Thermodynamics and Flow in Turbomachines. John Wiley & Sons, Inc., 1960.

15. Katsanis, Theodore: FORTRAN Program for Calculating Transonic Velocities on a Blade-to-Blade Stream Surface of a Turbomachine. NASA TN D-5427, 1969.

16. Meitner, Peter L.: FORTRAN Program for Calculating Coolant Flow and Metal Temperatures of a Full-Coverage-Film-Cooled Vane or Blade. NASA TP-1259, 1978.
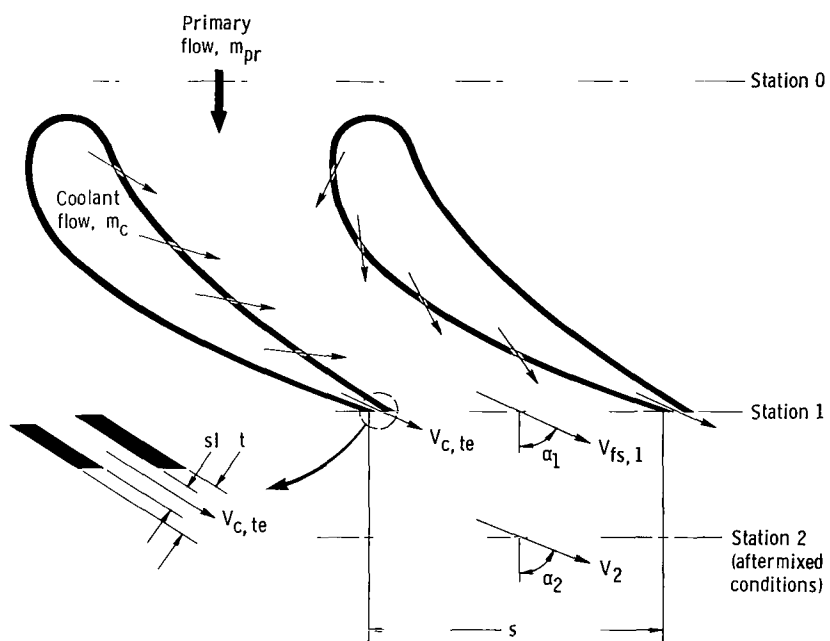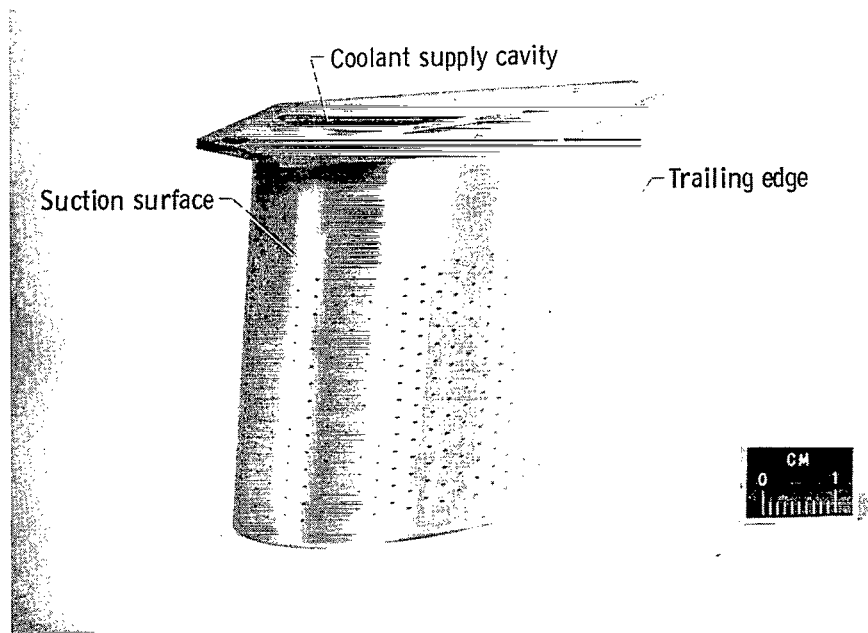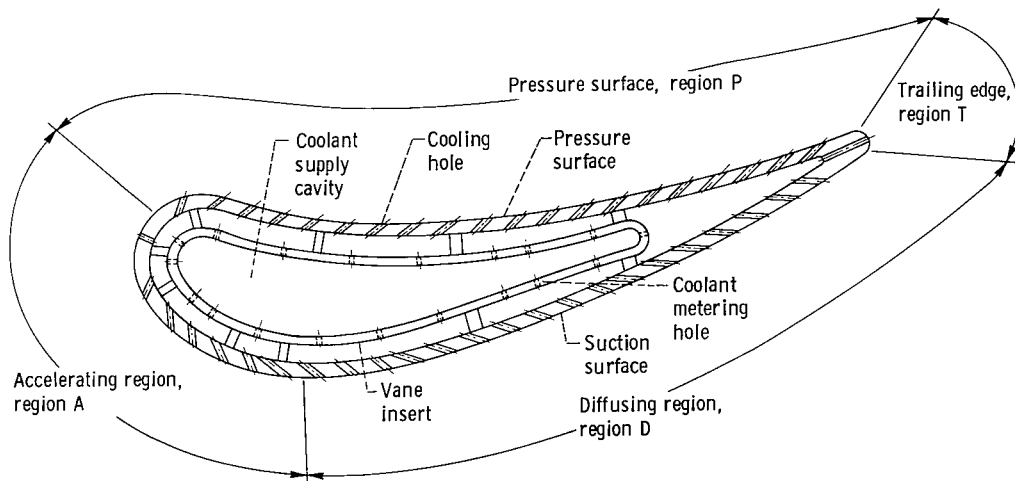
Figure 1. – Schematic of film-cooled vane, showing nomenclature.

(a) Test vane.

(b) Cross-sectional view of vane.

Figure 2. – Core turbine vane.

34
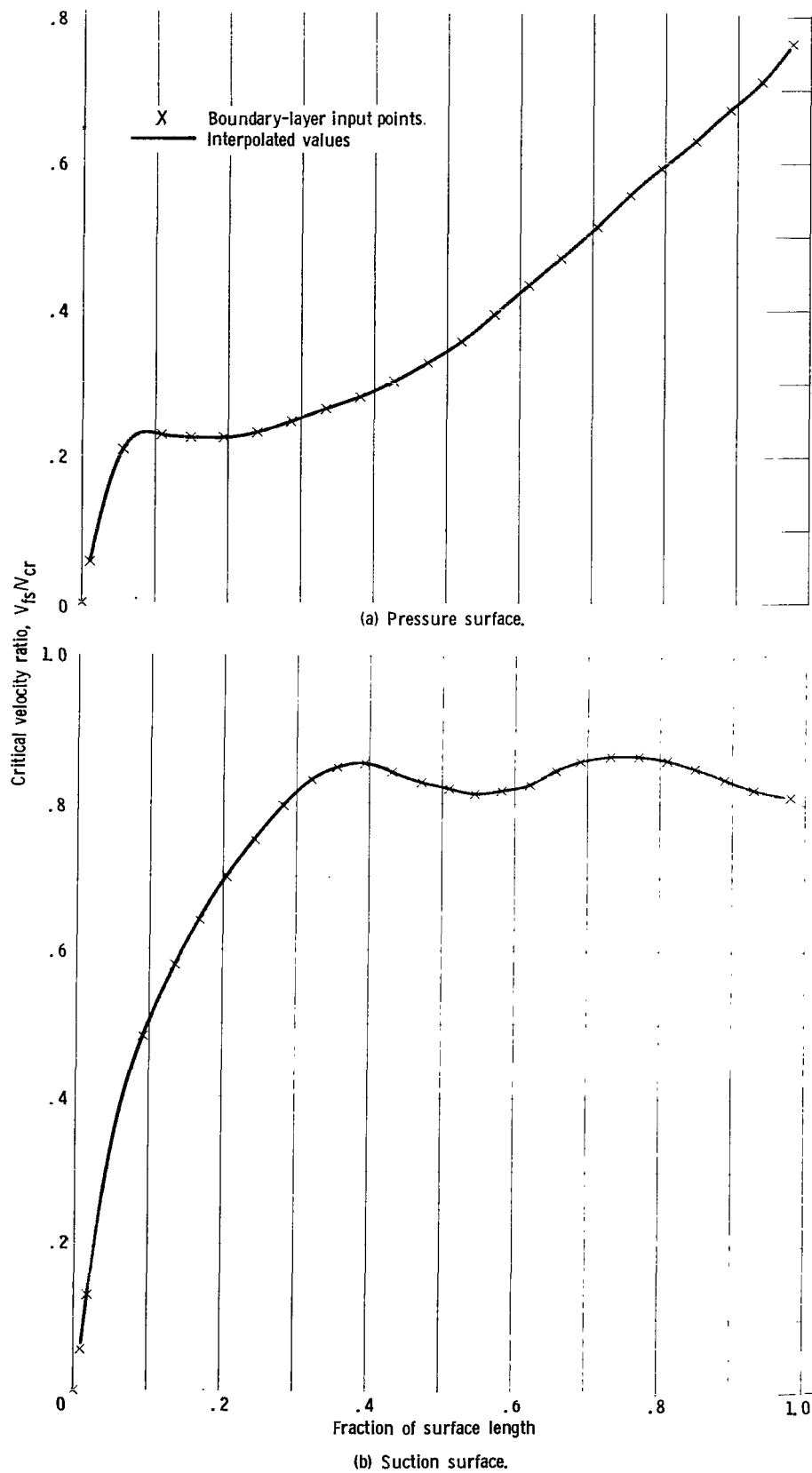
Figure 3. - Free-stream critical velocity ratio as a function of fraction of vane surface length.

35

(a) Solid (uncooled) vane, S.

(b) Fully cooled pressure surface, region P.
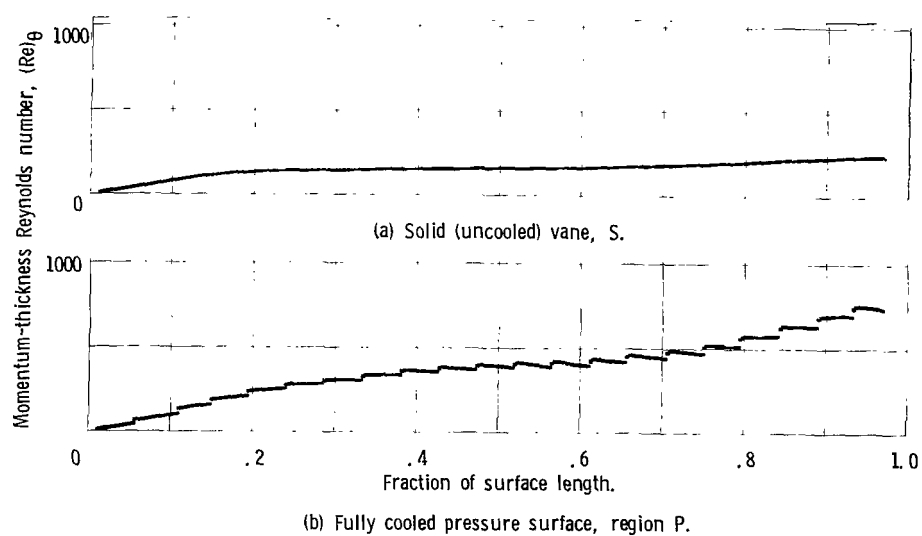
Figure 4. - Pressure-surface, momentum thickness Reynolds number for vane configurations tested at a total temperature ratio of 1.
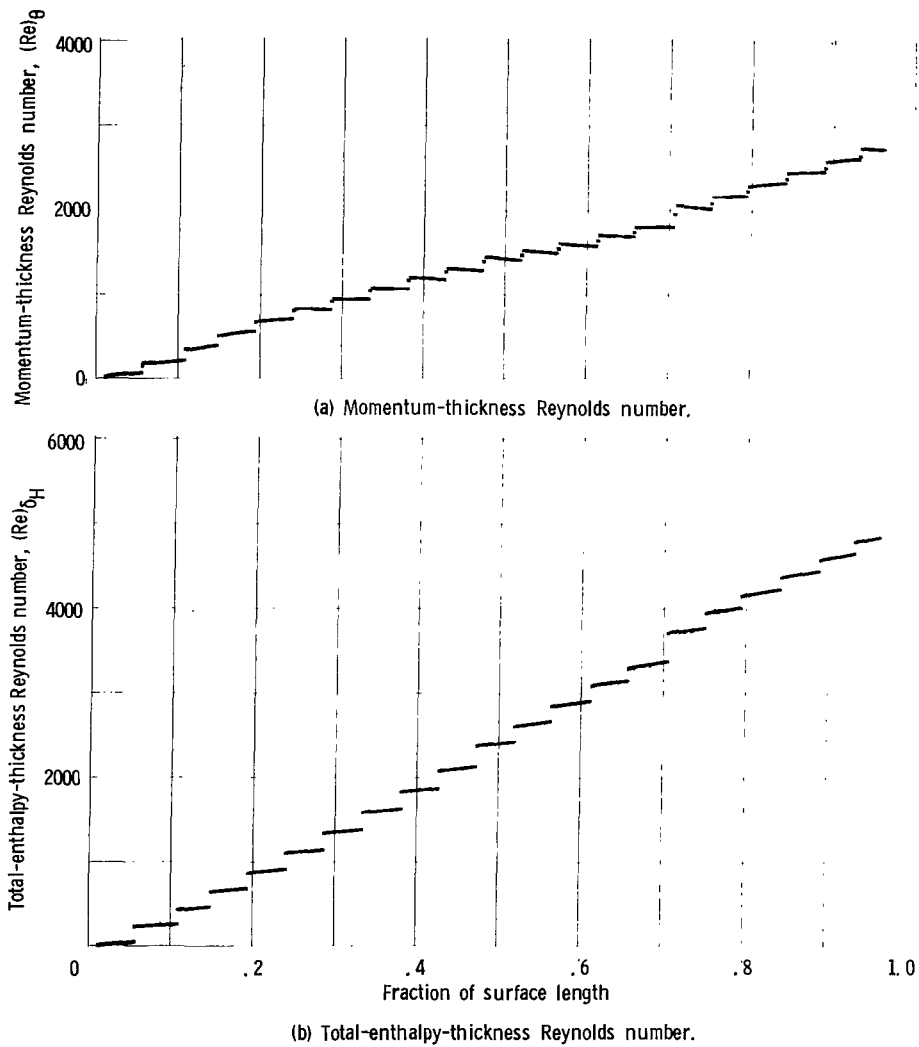
(a) Solid (uncooled) vane, S.

(b) Cooled accelerating region, region A.
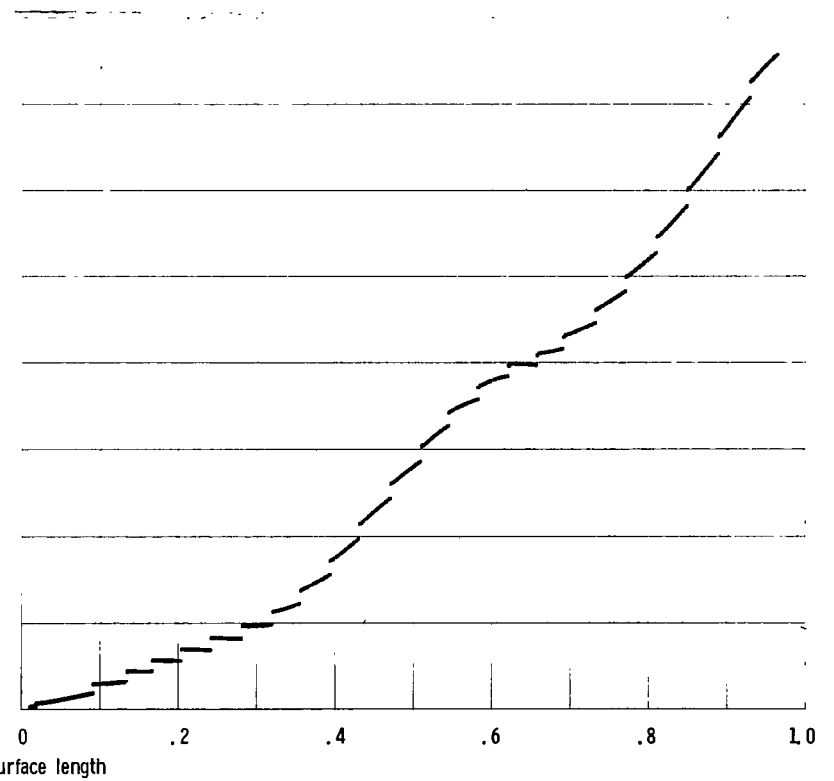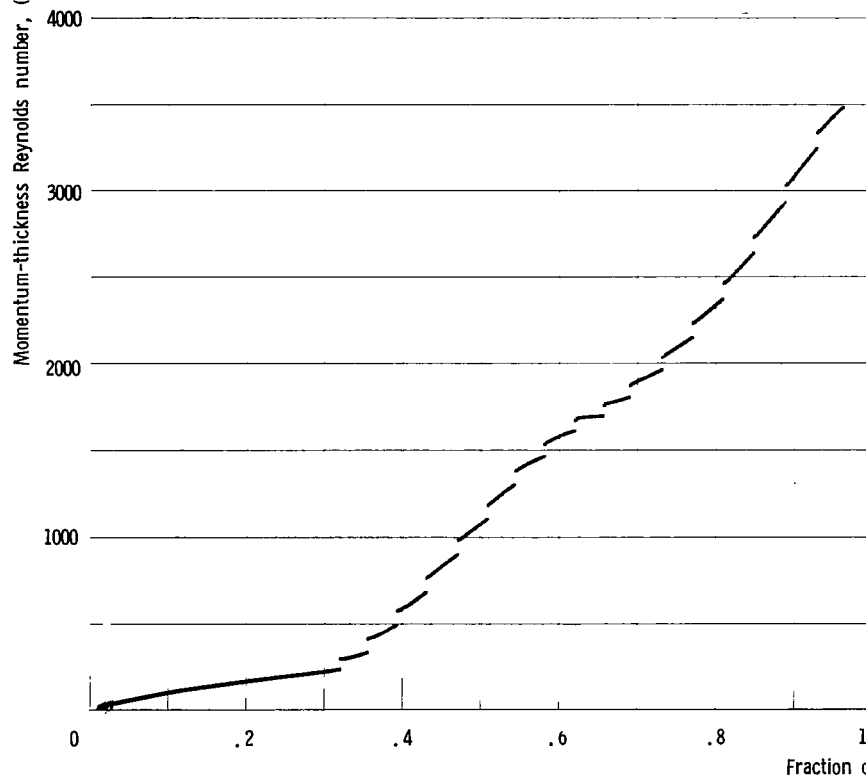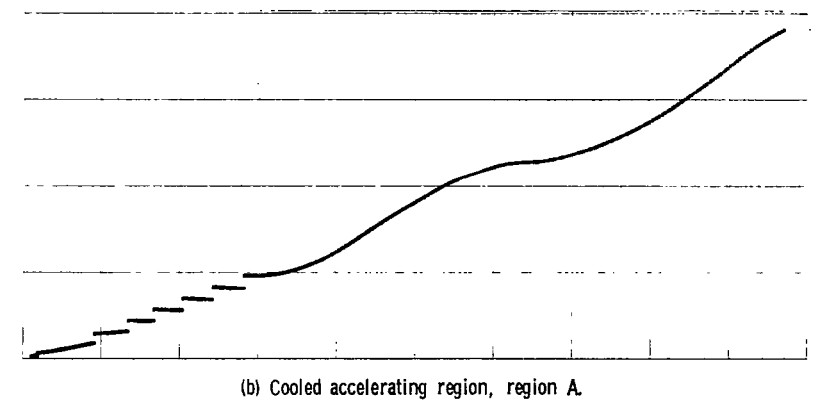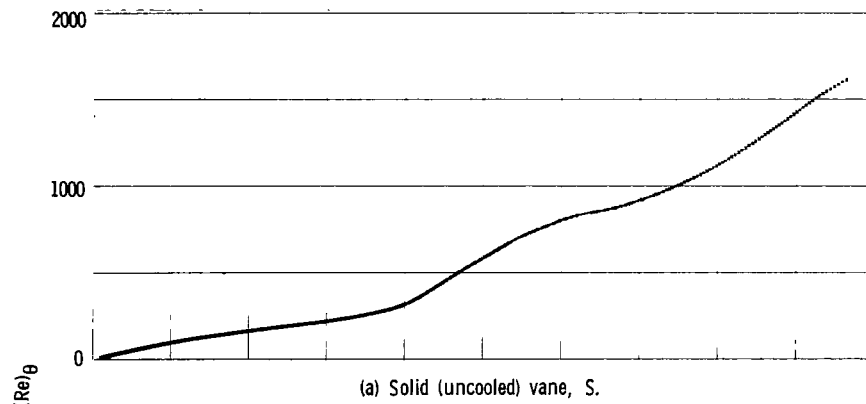
(c) Cooled diffusing region, region D.

(d) Cooled full suction surface, region AD.

Figure 5. – Suction-surface, momentum-thickness Reynolds number for vane configurations tested at a total-temperature ratio of 1.
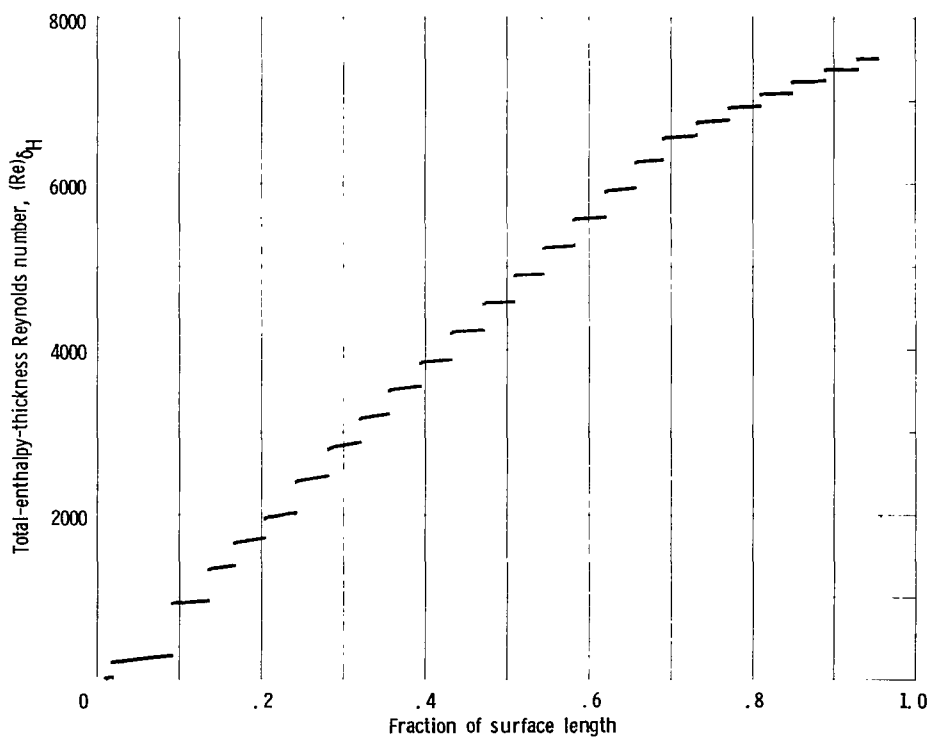
(a) Momentum-thickness Reynolds number.

(b) Total-enthalpy-thickness Reynolds number.

Figure 6. - Pressure-surface momentum and total-enthalpy-thickness Reynolds numbers for cooled vanes tested at a total-temperature ratio of 2.7.
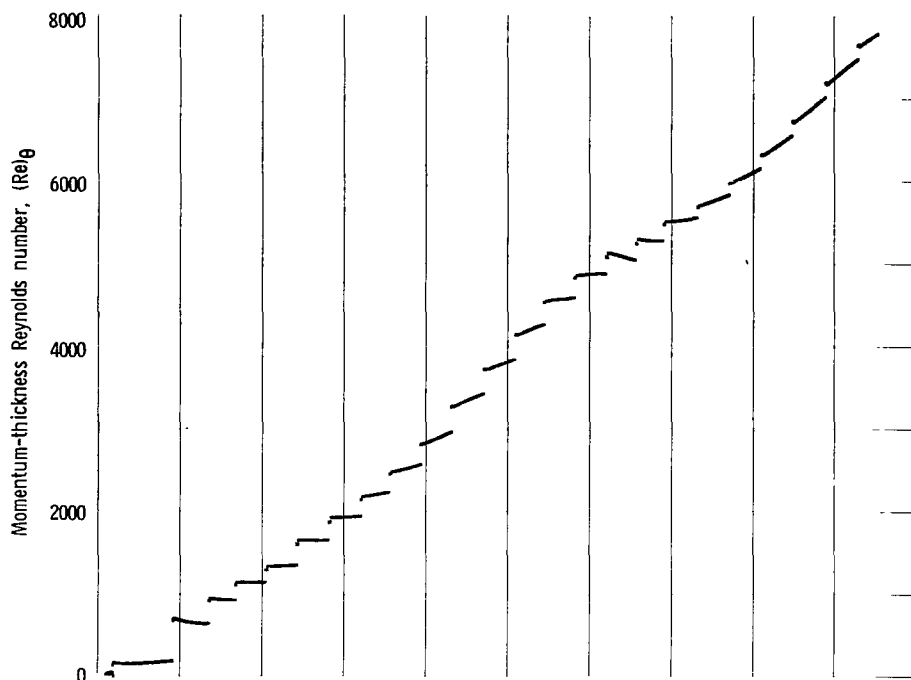
(a) Momentum-thickness Reynolds number.

(b) Total-enthalpy-thickness Reynolds number.

Figure 7. - Suction-surface momentum and total-enthalpy-thickness Reynolds numbers for cooled vanes tested at a total-temperature ratio of 2.7.
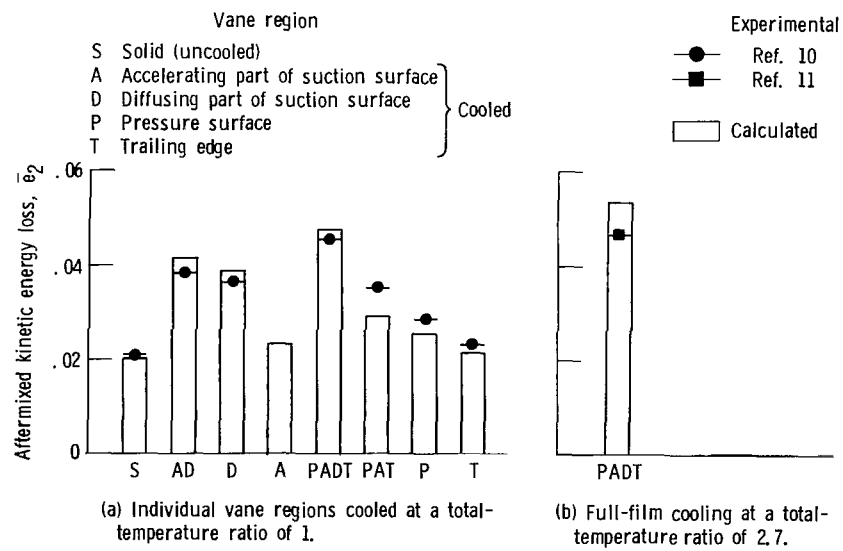
39

Figure 8. – Aftermixed kinetic energy loss for film-cooled vanes.

1. Report No. NASA TP-1623	2. Government Accession No.	3. Recipient's Catalog No.
4. Title and Subtitle PREDICTION METHOD FOR TWO-DIMENSIONAL AERODYNAMIC LOSSES OF COOLED VANES USING INTEGRAL BOUNDARY-LAYER PARAMETERS		5. Report Date February 1980
		6. Performing Organization Code
7. Author(s) Louis J. Goldman and Raymond E. Gaugler		8. Performing Organization Report No. E-076
9. Performing Organization Name and Address National Aeronautics and Space Administration Lewis Research Center Cleveland, Ohio 44135		10. Work Unit No. 505-04
		11. Contract or Grant No.
12. Sponsoring Agency Name and Address National Aeronautics and Space Administration Washington, D.C. 20546		13. Type of Report and Period Covered Technical Paper
		14. Sponsoring Agency Code

15. Supplementary Notes

16. Abstract

A generalized analysis to predict the two-dimensional aerodynamic losses of film-cooled vanes by using integral boundary-layer parameters is presented. Heat-transfer and trailing-edge injection effects are included in the method. An approximate solution of the generalized equations is also presented to show more clearly the effect of the different boundary-layer and cooling parameters on the losses. The analytical predictions agree well with the experimental results, indicating that available boundary-layer calculations for cooled vanes are of sufficient accuracy to use in the prediction method.

| 17. Key Words (Suggested by Author(s)) Aerodynamic performance Cooled turbine vanes Integral boundary-layer parameters | 18. Distribution Statement Unclassified - unlimited STAR Category 02 | | |
| 19. Security Classif. (of this report) Unclassified | 20. Security Classif. (of this page) Unclassified | 21. No. of Pages 42 | 22. Price* A03 |

THIRD-CLASS BULK RATE

6   1 1U,A,   020880 S00903DS
DEPT OF THE AIR FORCE
AF WEAPONS LABORATORY
ATTN: TECHNICAL LIBRARY (SUL)
KIRTLAND AFB NM 87117

NASA

POSTMASTER: If Undeliverable (Section 158
                Postal Manual) Do Not Return